Do Directionality Effects Influence Expected Damage?

A Case Study of the 2017 Central Mexico Earthquake

Luis A. Pinzón[a]*, Luis G. Pujades[a], Sergio A. Diaz[b], and Rodrigo E. Alva[a]

[a] Department of Civil and Environmental Engineering, Universitat Politècnica de Catalunya, Barcelona, Spain

[b] Academic Division of Engineering and Architecture, Universidad Juárez Autónoma de Tabasco, Tabasco, Mexico

*Contact information of corresponding author:

Luis A. Pinzón, M.Sc.

Address: Campus Nord-UPC, C. Jordi Girona 1-3, Building D2 303, 08034, Barcelona, Spain

Mobile phone: (+34) 654 020 581

Email: luis.pinzon@upc.edu

Other information:

Luis A. Pinzón (orcid.org/0000-0003-3128-7158)

Luis G. Pujades (orcid.org/0000-0002-2619-0805)

Sergio A. Diaz (orcid.org/0000-0003-3736-9154)

Rodrigo E. Alva (orcid.org/0000-0002-4522-3967)

Abstract

We analyze the case of a building that collapsed in a multifamily complex of Tlalpan borough in Mexico City during the 19 September 2017 Central Mexico earthquake. Despite having similar materials and similar structural and geometric properties, this was the only building that collapsed in the complex. A structural analysis of the building and a study of the soils' predominant periods indicated that resonance effects, if any, would not be significant. However, phenomena related to the anomalous performance of buildings in dense urban areas, such as geological soil, soil-structure interaction, and soil-city interaction effects were also investigated. A detailed analysis of the directionality of seismic actions recorded at nearby accelerometric stations and of the azimuths of sound and damaged buildings pointed to directionality effects as responsible for the collapse of the building.

Subsequently, a set of fifty-eight, two-component acceleration records of the earthquake in the city was used to perform a thorough directionality analysis. The results were then compared with the foreseen uniform hazard response spectra and the design spectra in the city. Seismic actions in the city due to this earthquake were stronger than those corresponding to the uniform hazard response spectra. In addition, although design spectra have been significantly improved in the new 2017 Mexican seismic regulations, they were exceeded in eleven of the fifty-eight analyzed spectra. In four of these eleven cases, the design spectra were exceeded due to directionality effects. These results confirm the necessity of considering directionality effects in damage assessments, in strong motion prediction equations, and in design regulations.

Introduction

The 19 September 2017 Central Mexico earthquake seriously affected Mexico City. In a multifamily complex belonging to the Civil Service Social Security and Services Institute (ISSSTE) in the Tlalpan borough, interestingly enough, only one building collapsed within a cluster of constructions that had the same structural typology, geometry, and materials. Similar facts were reported (Vargas-Alzate et al., 2018) in the San Fernando neighborhood, during the 2011 Lorca earthquake in Spain. During field work after earthquakes, it is not rare to find collapsed buildings that have the same structural properties as other undamaged, standing buildings nearby. An easy explanation would be that the collapsed building suffered from construction faults, which severely affected its seismic capacity and strength. However, it is well-known that the intensity of ground motion may vary significantly from site-to-close site and is not uniform in all directions, so other effects could significantly increase the seismic actions withstood by specific buildings, thus increasing the damage in comparison with nearby buildings. These effects are analyzed in this paper. First, a structural analysis of the building is performed to determine its modal-eigen properties. Several potential amplification effects due to soil-structure and soil-structure-soil (city-site) interaction are analyzed. Subsequently, attention is paid to directionality as the most likely effect explaining the differences in damage observed. Finally, overall directionality effects of the strong motion data of the 19 September 2017 earthquake, recorded at the Accelerographic Network of Mexico City (see the Data and Resources Section) are also analyzed.

Mexico City and the 2017 Central earthquake

Seismic hazard in México City

Mexico City is a zone with high seismic hazard due to the following conditions: i) the city is in a country where tectonic plates and active faults coexist. The Pacific coast is part of the Ring of Fire, which contains the most active seismic zones on Earth. In a seismicity study of the 20th century in Mexico, Kostoglodov and Pacheco (1999) found that, on average, there are five earthquakes of magnitude Mw ≥ 6.5 every four years. Every year, over a hundred earthquakes with Mw ≥ 4.5 are registered. In the 21st century, 72 earthquakes with Mw ≥ 6 have been reported; ii) soft soils therein strongly amplify the seismic waves. These conditions were clearly highlighted during the 1957 (Mw = 7.7) and 1985 (Mw = 8.1) earthquakes. Since then, the conditions of Mexico City have been the object of study (Singh et al., 1988; Chávez-García and Bard, 2004).

The 2017 Central Mexico earthquake

Like the dates of the 28 July 1957 and 19 September 1985 earthquakes, the 19 September 2017 is a day that no Mexican will forget. An earthquake of magnitude Mw = 7.1 on the Richter scale occurred, exactly 32 years after the 1985 Mexico City earthquake. The earthquake was reported as an intraplate event, in the

Cocos oceanic plate, at a depth of 57 km and with an epicenter close to 120 km from Mexico City (data from the Mexican Seismological Service, SSN-UNAM).

The Civil Protection in the Mexican Ministry of the Interior (SEGOB) (see Data and Resources) reported 369 fatalities caused by the event (228 in Mexico City, 74 in Morelos, 45 in Puebla, 15 in Mexico State, 6 in Guerrero, and 1 in Oaxaca). Regarding structures, 38 collapsed buildings were reported in Mexico City. Although this earthquake had one degree less magnitude than the 1985 earthquake (in other words, it was 32 times smaller), a high amount of structural damage was reported. This catastrophic situation was attributed to the fact that the earthquake hypocenter was much closer than that of the 1985 earthquake (400 km approx.). Moreover, a different frequency band was excited. The 1985 event had the greatest effect on zones with soft soils (with longer resonant periods), whereas this event generated greater acceleration in the transition zones where the predominant periods of the soils are shorter. These effects can be seen in Figures 1 and 2, in which the response spectra of the horizontal components of both earthquakes are shown and compared. The response spectra correspond to very close stations that have the same type of soil. In Figure 1, the values for short periods of approximately 0.5 seconds show an amplification in the spectral response for the 2017 earthquake.

Both stations are in the transition zones, so it can be observed clearly that the 2017 event had a greater effect in this area than that of the 1985 event. In Figure 2, the response spectra for the horizontal components of two stations with very soft soil (seismic zone III C, according to the Mexico City seismic codes) are presented, showing that the 1985 earthquake generated higher spectral accelerations than the 2017 earthquake.

The case of the Tlalpan 1C building

The building identified as 1C is part of the ISSSTE multifamily complex development consisting of 11 masonry mid-rise buildings (Figure 3). The 1C building has the same structural typology, geometry, and materials as another six buildings in the complex (2A, 2B, 2C, 4A, 4B and 4C). However, this building was the only one that collapsed on the site (see Figure 3b). According to official reports, buildings 2A, 3A and 3C did not suffer significant damage, buildings 2B, 2C, 3B, 1A, 1B, 4A, 4B and 4C suffered repairable damage, and building 1C collapsed at higher levels.

The studied building had six stories and contained 30 apartments. The first level was dedicated to offices and commerce. The shape of the building was rectangular (7.7 × 56.4 m) and 12.8 m high. The structure used orthogonal confined hollow brick masonry walls as seismic resistant elements and reinforced concrete slabs as horizontal diaphragms.

The complex is located within transition seismic zone II in the south of Mexico City; 113.5 km from the epicenter. Buildings in the complex were designed and constructed according to the Mexican State Construction Code of 1942 with a seismic coefficient of 0.025 (see the MSCC 1942 for details on this coefficient). The construction was completed in 1957 after the earthquake of the same year (7.7 Mw) and no major damage due to that earthquake or the earthquake of 19 September 1985 were documented.

Structural analysis

To evaluate the amplification and other effects that could affect the structural behavior of the Tlalpan complex, a 3D model was developed. The plans of the 1C building and SAP2000 software (see Data and Resources) were used. Figure 4 shows a sketch of the building.

The weak and strong axes are depicted. First, a modal analysis was performed to obtain the modal properties of the building. The period and mass participation factors for each mode are shown in Table 1. The predominant periods obtained in the weak and strong axes were 0.30 and 0.25 s respectively. A dynamic analysis (time history) was also performed, using the ground motions from stations DX37 and AO24. The records from these stations were used due to their proximity to the building complex. The analysis was performed taking into account the orientation of the buildings (see Figure 3) assigning their corresponding rotated ground-motion pairs according to the following azimuths: 344° (1C), 294° (2A, 2B and 2C), and 254° (4A, 4B and 4C).

The peak parameters, base shear (F), and roof displacement (δ) obtained in the dynamic analysis are shown in Table 2. The results show maximum values in the weak axis of the 1C building in both analyses. The overall maximum was obtained through the analysis performed with the closer station DX37. This gave values of 8249 kN of base shear and 0.87 cm of roof displacement for the weak axis of the collapsed building (1C).

Inter-story drifts and shears in each story were estimated for the buildings 1C and 4 (A, B and C) (see Figure 5).

The weak axis of the 1C building had the maximum inter-story drifts and shears in each story. Moreover, the inter-story drifts indicated that the base plant was less deformed, due to its higher rigidity, and show why the upper stories collapsed while the first floor remained intact (pictures of the damage reported in the buildings of the complex after the earthquake can be seen in the reports; see Data and Resources). The structural analysis allowed us to identify a brittle type failure observed in the stories above the first floor due to the mechanical properties of the structural typology, that is, a low-ductility masonry building. Thus, the building would collapse with relatively small displacements (Sucuoglu and Erberik, 1997; Bothara et al., 2010). Effects of stiffness irregularity and strength discontinuity in elevation were also seen. These effects were due to the abrupt change in column size in the first floor and above, increasing the inter-story drift in the first story (the soft story effect). In addition, a short-column effect, due to the window openings was observed; this effect amplifies the moment demand in the first story. All these effects become relevant when seismic action is applied to the building, altering the structural behavior and increasing the risk of collapse.

Phenomena related to anomalous performance of buildings

Several site effects, concerning both the soil geology and the structure itself, may influence the seismic actions beneath buildings (Menglin et al., 2011) and, therefore, might be responsible for anomalous seismic responses and performance. Relevant, well-known effects that alter input ground motions are: i) geological/geotechnical soft soil (GSS), ii) soil-structure interaction (SSI) (Guéguen et al., 2000; Laurenzano et al., 2010), iii) site-city interaction (SCI) (Guéguen et al., 2002, 2012; Kham et al., 2006; Semblat et al., 2008), and iv) directionality effects. In this section, these effects are described and discussed to determine which of them could be responsible for the response of the 1C building.

Geological soft soil (GSS) effects

The geological characteristics of the site affect the frequency content and duration of ground motions. This is a well-known effect, and seismic codes allow for it by means of soil classes. Depending on the thickness, geometry, and geotechnical properties of the soil deposits, soft-soils amplify free-field motions in the long-period range (Elnashai and Di Sarno, 2008). Then, the closeness between amplified periods of soils and fundamental periods of buildings would cause the effect known as site resonance. Thus, from information on the soil's amplification frequencies and on fundamental periods of vibration of the buildings, likely resonant effects can be detected. There are many techniques and procedures to deal with soft soil transfer functions. Several methods are based on spectral ratios, using both microtremor and earthquakes. Below, the predominant periods of the soils in the site are estimated, to investigate whether soil effects could be responsible for the anomalous response of the 1C building. The available historic strong-motion data recorded at the three closest stations (DX37, CH84 and AO24) were collected and analyzed. The H/V spectral ratio method proposed by Zhao et al. (2006) was then used to estimate the predominant site periods. Figure 6 shows the results obtained at each station. For the DX37 and AO24 stations, a predominant period of T = 1.0 s was obtained, and a value of 1.3 s was obtained for the CH84 station.

Moreover, a Mexico City structural code application SASID (NTCDS-RCDF, 2017) enabled us to obtain the predominant periods of soils in these sites. The values obtained with SASID are in good agreement with those obtained with H/V ratios (Table 3).

The site fundamental period of the Tlalpan complex was also estimated. We obtained a value of T = 0.95 s, which is close to that corresponding to strong-motion stations DX37 and CH84. Notably, the geotechnical report after the September 2017 earthquake (see Data and Resources), declared uniformity in the soil underneath the buildings. Therefore, the same site predominant period (T = 0.95 s) was considered for the entire complex. The periods of the buildings in the area (see Table 1) are far from these amplifying periods, thus making it unlikely that soil effects could be responsible for the bad response of the 1C building.

Soil-structure interaction (SSI)

Soil structure interaction (SSI) can be defined as the coupling between a structure and its supporting medium during earthquakes (Thusoo et al., 2015). Often, this effect can be seen in structures built on soft-soils (Bard et al., 2005) and it was responsible for a dramatic increase in the damage on the Hanshin expressway in the Kobe earthquake (Mylonakis et al., 2000). However, until a few years ago, seismic codes ignored the SSI effect on the seismic demand on buildings, based on the consideration that SSI effects reduce demands on structures, so that it is more conservative to apply conventional structural regulations. However, recent work has shown that it is not always conservative to ignore SSI (Givens, 2013). SSI modifies the free-field ground motions due to inertial and kinematic interaction effects. The SSI effect concerns the joint response of three connected systems: the structure, the foundations, and the soil underlying and surrounding the foundations. These three connected systems modify the building and foundation responses and the free-field seismic actions (Tuladhar et al., 2008).

The NIST GCR 12-917-21 (2012) report synthesizes the state-of-the-art of SSI and provides guidelines and techniques for simulating and modeling SSI effects in engineering practice. In this report, the structure-to-soil stiffness ratio, $r = h/(V_s T)$, is suggested as a relative measure for determining when SSI effects may become significant. *h* is the effective height to the center of mass for the first mode shape, V_s is the effective shear wave velocity, and T is the period of the fundamental mode of vibration. Values of r above 0.1 would indicate that SSI effects should be considered. From the available information (see the Data and Resources section), $h = 8.6$ m and $V_{s\,av} = 475$ m/s, and soil class C (according to FEMA [2004]) have been obtained for the 1C building, so that the r values for periods 0.30 and 0.25 (see Table 1) are 0.06 and 0.07 respectively. Because these ratios are less than 0.10, strong inertial SSI effects are not expected. In any case, due to the similarity of the structural and soil properties of the buildings in the complex, SSI effects would not explain the singularly bad performance of the 1C building.

Site-city interaction (SCI)

In dense urban areas subjected to strong seismic actions, the multiple interactions between soil, layers, and buildings is known as the site-city interaction (SCI) effect. SCI effects appear when there is resonance between buildings and soils. Building density and regular or irregular city configurations play a crucial role in energy distribution inside the city (Guéguen et al., 2002, 2012; Semblat et al., 2002, 2004, 2008; Kham et al., 2006; Bard et al., 2005). SCI in cities with a regular configuration reduces the top motion of buildings with respect to the single-building case and significantly reduces the ground motion inside the city. In several cases, the energy of the ground motion may be reduced by 50%. On the contrary, ground motion may increase outside the city; the energy radiated outside the city may involve about 10% of the free-field motion (Kham et al., 2006). In the case of irregular dense distributions of buildings, the coherency among the building responses diminishes resulting in a stronger decrease in the spatial correlation of the ground motion. This loss of coherency may result in constructive interference that could produce local peaks, in which the site-to-site energy variability may reach 50% (Kham et al., 2006). Therefore, despite there being no resonance conditions in the Tlalpan residential complex, SSI effects could not be fully discarded. A more detailed analysis would require more high-quality data and information, and is beyond the scope of this study.

Because directionality effects emerged as the factor that was probably responsible for the anomalous performance of the 1C building, these effects were analyzed in more detail. The influence of the azimuth of the buildings on the expected damage and the directionality effects in the response spectra are analyzed below.

Directionality effects

Directionality effects in seismic actions are evaluated by rotating the two horizontal orthogonal as-recorded ground motions, usually $acc_{E\text{-}W}$ and $acc_{N\text{-}S}$, according to the following equation:

$$\begin{matrix} accx(\theta) \\ accy(\theta) \end{matrix} = \begin{bmatrix} \cos(\theta) & \sin(\theta) \\ -\sin(\theta) & \cos(\theta) \end{bmatrix} \begin{bmatrix} acc_{N-S} \\ acc_{E-W} \end{bmatrix} \; \theta = 0°, 1°, \ldots N° \qquad (1)$$

where θ is the rotation angle and N is usually 180º. Equation (1) allows us to obtain new acceleration time histories, $acc_x(\theta)$ and $acc_y(\theta)$, in a θ-rotated reference system. Peak ground accelerations (PGA) and acceleration response spectra, Sa (T), for any given period, T, are strongly influenced by the orientation of the recording sensors. The influence of this on the ground-motion prediction equations (GMPE) and on the expected damage of a structure is well-known. A number of studies have analyzed these effects on seismic hazard (Watson-Lamprey and Boore, 2007; Boore and Kishida, 2016; Haji-Soltani and Pezeshk, 2017), on how the angle of incidence of the seismic action influences the performance of a structure (Lagaros, 2010; Torbol and Shinozuka, 2014; Vargas-Alzate et al., 2018) and on the horizontal-to-vertical spectral ratios of micrometers (Matsushima et al, 2017).

Effects on the 1C building

Ground motions may be polarized so that the intensity in a specific direction may be significantly greater. Moreover, as pointed out above (see Figure 4), most of the buildings have strong and weak axes, which depend on the rigidity or flexibility of the building in the directions defined by its principal axes (see Figure 7a). Therefore, a specific ground motion can have a greater effect on the performance of a building, depending on the orientation of these axes with respect to the action. Thus, the demand on the structure may strongly depend on the orientation of the building with respect to the direction in which the maximum intensity of the seismic action occurs, that is, depending on the azimuth of the building (see for instance Huang et al., 2008 and Vargas-Alzate et al., 2018). Figure 7b illustrates how the impact of a unitary force varies depending on the orientation of the building. Therefore, the expected damage would depend on the combined effects of the directionality of the seismic actions and the azimuthal orientation of the building. Accordingly, the expected damage will be greater when the strongest seismic forces hit the building in the weak axis direction.

Noticeably, the 1C building was the only one that collapsed in the Complex (Figure 3b), and, among the buildings with the same geometrical and structural properties it was the only one whose weak axis had an azimuth of 164°, measured from the south (Figure 8). To try to find an explanation for this fact, a thorough analysis of the seismic actions that could likely hit the building was made. For this purpose, the accelerograms recorded at the three closest stations were analyzed (see Figure 9); namely AO24 (2.52 km), DX37 (0.70 km), and CH84 (1.98 km). As a first step, the particle motion during the earthquake in these three stations was displayed (Figure 10). For the closest station, DX37, a maximum acceleration of 196 cm/s^2 was found at an azimuth of 165° measured from the south. This angle is very close to the orientation of the weak axis of the 1C building. This suggests that the building was probably more affected by the earthquake due the combined effects of the directionality of the seismic action and the orientation of its weak axis. The other buildings in the complex were clearly subjected to similar accelerations, but the strongest acceleration did not directly affect their weak axes. Similar results were obtained from strong motion data from the other two stations, CH84 and AO24 (Figure 10). A similar phenomenon was also observed and studied in Lorca, Spain, after the 5.1 Mw magnitude earthquake of 11 May 2011 (Vargas-Alzate et al., 2018).

The PGA and the maximum responses of a single degree of freedom 5% damped oscillator with a period of 0.30 s were also analyzed as functions of the rotation angle. Figure 11 shows the results. The orientations of the weak axis of each building are also shown. Azimuths of 74º and 114º, measured from the south, correspond to the directions of the weak axes of buildings 4 (A, B and C) and 2 (A, B and C) respectively. It can be seen how maximum values of PGA and of the acceleration response of a 5% damped system with a period of 0.3 s were obtained very close to the 164º orientation of the weak axis of the 1C building (see Figure 8), which, accordingly, bore the most unfavorable seismic action. The other buildings in the complex clearly received smaller accelerations in their weak axis.

Ground motions and design spectra

Conscientiousness and awareness of the influence of directionality effects on ground motions and ground motion prediction equations (GMPE) have increased in recent decades (see for instance Boore et al., 2006; Abrahamson et al., 2008; Boore, 2010; Shahi and Baker, 2014; Bradley and Baker, 2015; Boore and Kishida, 2016). The GMRotI50 Sensor-orientation-independent measure, as proposed by Bore et al. (2006), was considered for the Next Generation Attenuation-West project (NGA-West, Abrahamson et al., 2008); In the GMRotIpp intensity measure, GM stands for geometric mean, Rot for rotation, I for period-independent, and pp corresponds to the pp-percentile. Later, in 2012, the projects NGA-West2 (Bozorgnia. et al., 2012; Shahi and Baker 2014) and NGA-East (PEER 2015) used the 50^{th} percentile (pp=50) of the Rotation Dependent measure (RotDpp), proposed by Boore (2010), to update these GMPEs. For existing GMPE worldwide see Douglas (2018). Regarding structural regulations, the ASCE/SEI 7-10 (ASCE, 2010) adopted the measure RotD100 in the ground-motion design maps. These types of updates are of fundamental importance and they must be considered for a proper definition of the seismic hazard.

In this section, the directionality effects of the 2017 earthquake in Mexico City are analyzed. The results are then compared with the design spectra. In addition to the as-recorded accelerograms, the intensity measures (IM) described in Table 4 are used.

Fifty-eight ground motion (N-S and E-W) pairs, which were supplied by the Accelerographic Network of Mexico City, were selected for the directionality analysis. For comparison purposes, we used the design spectra of the structural design codes for Mexico City, published in 2004 (NTCDS-RCDF, 2004) and more recently in 2017 (NTCDS-RCDF, 2017). With respect to the 2004 regulations, the elastic design spectra without reduction factors were used, both those published in the main section and the alternative method proposed in Appendix A. In addition, the uniform hazard spectrum for each station was added to the comparison. To this end, the SASID A v4.0.2.0 application that proposes the new structural regulation was used (NTCDS-RCDF, 2017).

To assess the directionality effects, the 58 ground motion pairs were rotated (Equation 1) and their respective 5% damped response spectra were obtained. The rotation was made for the range between 0° and 180°, with increments of $\theta = 1°$. Finally, the RotD100 spectrum was estimated. This spectrum represents the maximum spectral acceleration generated for each 5% damped single-degree-of-freedom oscillator system. From the comparison of the spectra, it was found that the elastic design spectrum of the 2004 regulation was not exceeded in only 9 of the 58 stations. However, when the obtained spectra were compared with those provided in Appendix A of the same code, using an alternative method, the design spectrum was exceeded in 15 of the 58 acceleration time histories tested. Concerning the new structural regulations published in December 2017, in 11 of the 58 stations, the proposed elastic design spectrum was exceeded. This represents an improvement with respect to Appendix A of 2004, but several of the new design spectra were still surpassed. Another important point is that, in four of the 11 stations where the new regulation was exceeded, the excess was due to directionality effects (these results are summarized in the Appendix to this paper). The 11 stations where the newer design spectra were exceeded are in areas of stiff to soft soil, 4 in seismic zone I, 3 in zone II (transition), and 4 in zone IIIA. In the zones with softer soils (IIIB, IIIC and IIID), the design spectra were not exceeded at all. This fact agrees with the structural damage reported since most of the buildings that collapsed were in zones I, II and IIIA (see Data and Resources). Figure 12 shows the comparisons of the response spectra for 6 stations: 2 in zone I, 2 in zone II, and 2 in zone IIIA.

In the stations of zone I of stiff soil (Figure 12 a and b), the maximum spectral accelerations occurred for low periods, in the range from 0.3 to 0.6 s, and have a value that exceeds 500 cm/s^2 at the station CP28 and, approximately, 340 cm/s^2 at the station PA34. These spectral accelerations would affect relatively low buildings, those with roughly 3 to 6 stories. In zone II (Figure 12 c and d), spectral accelerations greater than 1 g were estimated at the DX37 station (Figure 12 c), for periods slightly greater than 1 second. Amplification in this period would affect buildings of approximately 10 floors. Finally, the highest spectral accelerations were obtained in the stations of the IIIA zone (Figure 12 e and f). A maximum spectral acceleration of 1600 cm/s^2 was obtained at Station CH84 for a period of approximately 1.4 seconds, and the maximum spectral acceleration at station JC54 was 1200 cm/s^2 for the same period.

Overall directionality effects

Finally, to evaluate IMs with respect to the maximum spectral acceleration (RotD100), ratios were estimated using N-S, E-W, Larger and GM measures (see definitions in Table 4). The E-W component had, on average, values closer to RotD100 than the N-S (see Figure 13). The ratio RotD100/GM had values between 1.20 and 1.30. When we evaluated the ratio of RotD100 with respect to the Larger measure, we observed differences of 10%, on average. These trends in the ratios were compared with the ratio RotD100/Larger (for earthquakes with 0 km < R_{RUP} ≤ 200 km and 7.0 ≤ M < 8.0) obtained by Boore and Kishida (2016) and the ratio RotD100/GM model proposed by Haji-Soltani and Pezeshk (2017). Very similar results were obtained for the ratio RotD100/Larger, while the ratios obtained herein for the RotD100/GM were slightly lower than that proposed by Haji-Soltani and Pezeshk.

Conclusions

We analyzed the anomalous seismic performance of a specific building in a multifamily residential complex in Tlalpan borough in Mexico City, during the 19 September 2017 earthquake of Mw=7.1. Soil, SSI, SCI, and directionality effects were investigated to find a reasonable explanation for such an inconsistent seismic response. The homogeneity of the soils and the similarity of the geometrical and structural properties of the buildings in the complex allowed us to discard soil, SSI, and SCI effects as causative of significant differences in the seismic actions suffered by the buildings. Thus, directionality effects emerge as the main cause. The concurrence of the orientation of the weak axis of the building and the direction at which the maximum demand of the seismic actions is attained would be responsible for the collapse of the building. Thus, in damage and risk assessments, the direction in which the strongest seismic actions hit the buildings, directionality, should be considered, as similar buildings, located in the same place, may suffer different damage grades.

Concerning seismic hazard, Figure 12 shows how the response spectra predicted by the SASID A v4.0.2.0 application (NTCDS-RCDF, 2017) are lower than those corresponding to the seismic actions produced by the 2017 earthquake. This fact confirms that it is important to incorporate the results of directionality studies into the GMPEs by means of sensor orientation-independent measures. Thus, epistemic uncertainties in GMPE would be significantly reduced, and the foreseen seismic actions would be more realistic. However, the consideration of maximum seismic actions could lead to excessively conservative GMPE. Therefore, the median values or specific percentiles should be considered. The use of acceleration time-histories that are compatible with the RotD100 measure in dynamic analysis of structures would allow the most unfavorable case to be analyzed. These extreme values could be adopted for the design and/or rehabilitation of special structures such as historical-cultural heritage buildings or other essential and special high-risk structures.

Regarding design spectra, seismic regulations in Mexico City have been improved in recent years. However, later design spectra were still surpassed by several accelerograms recorded during the September 2011 earthquake (see Tables A1 to A6 in the appendix). Noticeable, these excesses were due to directionality effects. Thus, an important conclusion of this study is that directionality effects must be considered in Probabilistic Seismic Hazard Analyses (PSHA), in damage assessments, and in design regulations. Specific studies on directionality effects should be performed in urban areas located in high seismic hazard zones. However, studies undertaken in other countries may be useful as the ratios RotD100/GM and RotD100/Larger, found in other studies, are comparable to those found in this study, in a wide range of periods.

Data and Resources

The ground-motion records used for this study were provided by the Centro de Instrumentación y Registro Sísmico (Instrumentation and Seismic Recording Center), Mexico, through the Red Acelerográfica de la Ciudad de México (Accelerographic Network of Mexico City) at http://www.cires.org.mx/ (last accessed on 19 May 2018). The reports and plans from the ISSSTE multifamily complex were obtained from the Secretaría de Obras y Servicios at http://www.obras.cdmx.gob.mx/uh-tlalpan (last accessed on 19 May 2018). A map with a summary of the damages due to the Central Mexico Earthquake is available at http://learningfromearthquakes.org/2017-09-19-puebla-mexico/data-map (last accessed on 19 May 2018). Figure 3 was obtained at http://unavidamoderna.tumblr.com/image/86044704110 (last accessed on 19 May 2018). The building structural model was numerically simulated using SAP2000 software (http://www.csiamerica.com/products/sap2000; last accessed 18 April 2018).

Acknowledgments

This research was partially funded by the Spanish Government's Ministry of Economy and Competitiveness (MINECO) and by the European Regional Development Fund (ERDF) of the European Union (EU) through the project referenced as CGL2015-65913-P (MINECO/ ERDF, EU). The first author is supported by a Ph.D. scholarship grant from the Institute for the Training and Development of Human Resources (IFARHU) and the Government of Panama's National Secretariat of Science, Technology, and Innovation (SENACYT). The fourth author is supported by a CONACyT scholarship.

References

Abrahamson, N. A, G. M. Atkinson, D. M. Boore, Y. Bozorgnia, K. W. Campbell, B. Chiou, I. M. Idriss, W. J. Silva, and R. R. Youngs (2008). Comparisons of the NGA ground-motion relations, *Earthq. Spectra* **24,** 45–66.

American Society of Civil Engineers (ASCE) (2010). Minimum design loads for buildings and other structures. ASCE/SEI 7-10, American Society of Civil Engineers/Structural Engineering Institute, Reston, VA.

Bard, P. Y., J. L. Chazelas, P. Guéguen, M. Kham and J. F. Semblat (2005). Site-city interaction, Chapter 5. pp 91-114, in Assessing and Managing Earthquake Risk, C. S. Oliveira, A. Roca and X. Goula (Editors), Springer, New York. 530 pp.

Beyer, K., and J. J. Bommer (2006). Relationships between median values and between aleatory variabilities for different definitions of the horizontal component of motion, *Bull. Seismol. Soc. Am.* **96,** 1512–1522.

Bradley, B. A., and J. W. Baker (2015). Ground motion directionality in the 2010-2011 Canterbury earthquakes, *Earthq Eng Struct Dyn* **44,** 371–384.

Boore, D. M. (2010). Orientation-independent, nongeometric-mean measures of seismic intensity from two horizontal components of motion, *Bull. Seismol. Soc. Am.* **100,** 1830–1835.

Boore, D. M., J. Watson-Lamprey, and N. A. Abrahamson (2006). Orientation-independent measures of ground motion, *Bull. Seismol. Soc. Am.* **96,** 1502–1511.

Boore, D. M., and T. Kishida (2016). Relations between some horizontal-component ground-motion intensity measures used in practice, *Bull. Seismol. Soc. Am.* **107,** 334–343.

Bothara, J. K., R. P. Dhakal, and J. B. Mander (2010). Seismic performance of an unreinforced masonry building: An experimental investigation, *Earthq. Eng. Struct. Dyn.* **39**, 45–68. doi: 10.1002/eqe.932

Bozorgnia, Y., N. A. Abrahamson, K. Campbell, B. Rowshandel, and T. Shantz (2012). NGA-West2: A comprehensive research program to update ground motion prediction equations for shallow crustal earth-quakes in active tectonic regions, Proc. of the 15th World Conf. on Earthquake Engineering, Lisbon, Portugal, 6 pp.

Chávez-García F. J, and P-Y. Bard (1994). Site effects in Mexico City eight years after the September 1985 Michoacan earthquakes, *Soil Dynamics and Earthquake Engineering* **13**(4), 229-247.

Douglas, J. (2018). Ground motion prediction equations 1964-2018. Department of Civil and Environmental Engineering. University of Strathclyde. Glasgow. UK. 609 pp.

Elnashai A.S. and L. Di Sarno (2008). *Fundamentals of earthquake engineering*, John Wiley&Sons, Ltd. Chichester, West Sussex. United Kingdom. 337 pp.

FEMA (2004). NEHRP recommended provisions for seismic regulations for new buildings and other structures (FEMA 450) Part 1: Provisions. 2003 Edition. Building Seismic Safety Council. National Institute of Building Sciences. Washington, DC.2004, 308 pp.

Givens, M. J. (2013) Dynamic Soil-Structure Interaction of Instrumented Buildings and Test Structures. PhD dissertation. University of California, Los Angeles, 367 pp.

Guéguen, P., P. Y. Bard, and C. S. Oliveira (2000). Experimental and numerical analysis of soil motions caused by free vibrations of a building model, *Bull. Seismol. Soc. Am.* **90**(6), 1464-1479.

Guéguen, P., J. F. Semblat, P. Y. Bard, and J. L. Chazelas (2012). Site-city interaction: Experimental and numerical approaches, *Bulletin des Laboratoires des Ponts et Chaussées* **279,** 35-46.

Guéguen, P., P. Y. Bard, and F. J. Chavez-Garcia (2002). Site-city seismic interaction in Mexico City like environments: an analytical study, *Bull. Seismol. Soc. Am.* **92**(2), 794–811.

Haji-Soltani, A., and S. Pezeshk (2017). Relationships among various definitions of horizontal spectral accelerations in Central and Eastern North America, *Bull. Seismol. Soc. Am.* **108**(1), 409–417.

Huang, Y., A. Whittaker, and N. Luco (2008). Maximum spectral demands in the near-fault region, *Earthq. Spectra* **24,** 319–341.

Kham, M., J. F. Semblat, P. Y. Bard, and P. Dangla (2006). Seismic Site–City Interaction: Main Governing Phenomena through Simplified Numerical Models, *Bull. Seismol. Soc. Am.* **96**(5), 1934-1951.

Kostoglodov, V., and J. F. Pacheco (1999). One hundred years of seismicity in Mexico, Inst. de Geofís., Univ. Nac. Autónoma de Mexico, Mexico City.

Lagaros, N. D. (2010). The impact of the earthquake incident angle on the seismic loss estimation, *Engineering Structures* **32**(6), 1577–1589.

Laurenzano, G., E. Priolo, M. R. Gallipoli, M. Mucciarelli, and F.C. Ponzo (2010). Effect of Vibrating Buildings on Free-Field Motion and on Adjacent Structures: The Bonefro (Italy) Case History, *Bull. Seismol. Soc. Am.* **100**(2), 802–818.

Matsushima, S., H. Kosaka, and H. Kawase (2017). Directionally dependent horizontal-to-vertical spectral ratios of micrometers at Onahama, Fukushima, Japan, Earth, Planets and Space 69, 96.

Menglin, L., W. Haifeng, X. Cheng and Z. Yongmei (2011). Structure-soil-structure interaction: Literature review, *Soil Dynamics and Earthquake Engineering* **31**, 1724-1731.

Mylonakis, G., G. Gazetas, S. Nikolaou, and O. Michaelides (2000). The role of soil on the collapse of 18 piers of the Hanshin expressway in the Kobe earthquake, Proc. of the 12th World Conference on Earthquake Engineering, Auckland, New Zealand. Paper n. 1074. 7 pp.

NTCDS-RCDF (2004). Normas Técnicas Complementarias para el Diseño por Sismo. Government of Mexico City, Mexico City.

NTCDS-RCDF (2017). Normas Técnicas Complementarias para el Diseño por Sismo. Government of Mexico City, Mexico City.

NIST GCR 12-917-21 (2012). Soil-structure Interaction for building structures. NEHRP consultants Joint Venture and National Institute of standards and Technology. US Department of Commerce. 292 pp.

PEER (2015). NGA-East: Median Ground-Motion Models for the Central and Eastern North America Region. PEER 2015/04. Pacific Earthquake Engineering Research Center, Berkeley, California. 351 pp.

Shahi S. K., and J. W. Baker (2014). NGA-West2 models for ground-motion directionality. PEER 2013/10. Pacific Earthquake Engineering Research Center, Berkeley, California. 73 pp.

Semblat, J. F., M. Kham, P. Guéguen, P. Y. Bard, and A.M. Duval (2002). Site-City interaction through modification of site effects, Proc. of the EERI. 7th US Conference on Earthquake Engineering, 2002, Boston, United States. 8 pp. CDROM.

Semblat, J. F., M. Kham, P. Y. Bard, and P. Guéguen (2004). Could “site-city interaction” modify site effects in urban areas?, Proc. of the 13th World Conference on earthquake engineering. Vancouver, BC. Canada. August 1-6, 2004. Paper No. 1978. 9 pp.

Semblat, J. F., M. Kham, and P. Y. Bard (2008). Seismic Wave Propagation in Alluvial Basins and Influence of Site-City Interaction, *Bull. Seismol. Soc. Am.* **98**(6), 2665-2678.

Singh, S. K., E. Mena, and R. Castro (1988). Some aspects of source characteristics of the 19 September 1985 Michoacan earthquake and ground motion amplification in and near Mexico City from strong motion data, *Bull. Seismol. Soc. Am.* **78**(2) 451–477.

Sucuoglu, H., and A. Erberik (1997). Performance Evaluation of a Three-Storey Unreinforced Masonry Building During the 1992 Erzincan Earthquake, *Earthq. Eng. Struct. Dyn.* **26**, 319–336.

Thusoo, S., K. Modi, R. Kumar, and H. Madarhar (2015). Response of buildings with soil-structure interaction with varying soil types, *International Journal of Civil and Environmental Engineering* **9**(4), 414-418.

Torbol, M., and M. Shinozuka (2014). The directionality effect in the seismic risk assessment of highway networks, *Structure and Infrastructure Engineering* **10**, 175–188.

Tuladhar, R., T. Maki, and H. Mutsuyoshi (2008). Cyclic behavior of laterally loaded concrete piles embedded into cohesive soil, *Earthq. Eng. Struct. Dyn.* **37**, 43–59. doi: 10.1002/eqe

Vargas-Alzate, Y. F., L. G. Pujades, A. H. Barbat, E. Hurtado, S. A. Diaz, and D. A. Hidalgo-Leiva (2018). Probabilistic seismic damage assessment of reinforced concrete buildings considering directionality effects, *Structure and Infrastructure Engineering* **14**(6), 817-829.

Watson-Lamprey, J., and D. M. Boore (2007). Beyond SaGMRotI: Conversion to SaArb, SaSN, and SaMaxRot, *Bull. Seismol. Soc. Am.* **97,** 1511–1524.

Zhao, J. X., K. Irikura, J. Zhang, Y. Fukushima, P. G. Somerville, A. Asano, Y. Ohno, T. Oouchi, T. Takahashi, and H. Ogawa (2006). An empirical site-classification method for strong-motion stations in Japan using H/V response spectral ratio, *Bull. Seismol. Soc. Am.* **96**, 914–925.

Authors' mailing addresses

Luis A. Pinzón, M.Sc.

Email: luis.pinzon@upc.edu

Address: Campus Nord-UPC, C. Jordi Girona 1-3, Building D2 303, 08034, Barcelona, Spain

Prof. Luís G. Pujades. Ph.D.

Email: lluis.pujades@upc.edu

Address: Campus Nord-UPC, C. Jordi Girona 1-3, Building D2 303, 08034, Barcelona, Spain

Sergio A. Diaz, Ph.D.

Email: sergio.alberto.diaz@upc.edu & alberto.diaz@ujat.mx

Address: Campus Nord-UPC, C. Jordi Girona 1-3, Building D2 303, 08034, Barcelona, Spain

Rodrigo E. Alva, M.Sc.

Email: rodrigo.esteban.alva@upc.edu

Address: Campus Nord-UPC, C. Jordi Girona 1-3, Building D2 303, 08034, Barcelona, Spain

Tables

Table 1 Modal properties, period (T), and mass participation factors (W) of the studied building.

Mode	Strong axis		Weak axis	
	T (s)	W (%)	T (s)	W (%)
1	**0.25**	0.71	**0.30**	0.68
2	0.08	0.15	0.21	0.18
3	0.03	0.09	0.10	0.12

Table 2 Maximum base shear (F in kN) and maximum roof displacements (δ in cm) generated in each building through the time-history analysis.

Ground-motion Station	1C building				2 (A, B, and C) buildings				4 (A, B and C) buildings			
	Weak axis		Strong axis		Weak axis		Strong axis		Weak axis		Strong axis	
	F	δ	F	δ	F	δ	F	δ	F	δ	F	δ
DX37	8249	**0.87**	5567	0.48	6339	**0.74**	5392	0.41	4629	**0.50**	6752	0.46
AO24	4953	**0.61**	3679	0.28	4891	**0.59**	3603	0.28	3406	0.41	4230	**0.47**

Table 3 Site fundamental periods obtained through SASID software and H/V response spectral ratio.

Site	Site period, T (s)	
	SASID	H/V ratio
DX37	0.8	1.0
CH84	1.3	1.3
AO24	1.0	1.0
Tlalpan complex	0.95	-

Table 4 Summary of ground motion IMs considered in this study.

IM symbol	Definition*
N-S, E-W	As-recorded horizontal orthogonal components.
GM	Geometric mean.
RotD100	Maximum (100th percentile) values of response spectra of the two as-recorded horizontal components rotated onto all non-redundant azimuths (Boore, 2010).
Larger	The larger of the two horizontal components (Beyer and Bommer, 2006; Bradley and Baker, 2015; Boore and Kishida, 2016).

* Definitions apply for peak ground acceleration (PGA) and for response spectral accelerations, Sa (T), which are functions of the period, T, of vibration.

List of figures

Figure 9. a) Epicentral distance from the 2017 Central Mexico earthquake to the 1C building. b) The three accelerographic stations closest to the 1C building site.

Figure 10. Particle acceleration motions at the three accelerometric stations closest to the 1C building site: (a) DX37 station, (b) CH84 station, and (c) AO24 station. The color version of this figure is only available in the electronic edition.

Figure 11. Variation of PGA and spectral acceleration, Sa, of a single-degree-of-freedom 5% damped oscillator with T=0.3 s as a function of the orientation angle, at DX37 accelerographic station. Vertical lines indicate the azimuths, measured from the south, to the weak axis of the 1 (C), 2 (A, B and C) and 4 (A, B and C) buildings. The color version of this figure is only available in the electronic edition.

Figure 12. Comparison of response spectra of records at different accelerometric stations in Mexico City, during the 2017 Central Mexico earthquake: (a) CP28 station [zone I], (b) PA34 station [zone I], (c) DX37 station [zone II], (d) EO30 station [zone II], (e) CH84 station [zone IIIA], and (f) JC54 station [zone IIIA]. The color version of this figure is only available in the electronic edition.

Figure 13. Comparison of the ratios RotD100/N-S, RotD100/E-W, RotD100/GM, and RotD100/Larger with ratios proposed by other researchers. The color version of this figure is only available in the electronic edition.

Figures

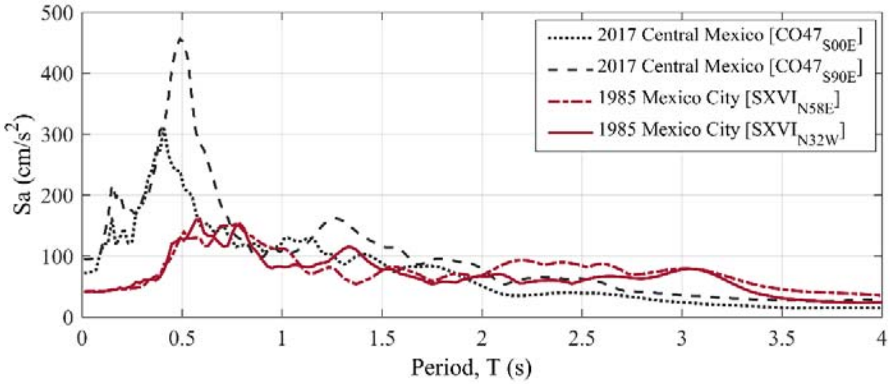

Figure 1. Comparison between the response spectra (5% damped) of the horizontal as-recorded components from the 1985 Mexico City earthquake (SXVI station – seismic zone II) and the 2017 Central Mexico earthquake (CO47 station – seismic zone II). The color version of this figure is only available in the electronic edition.

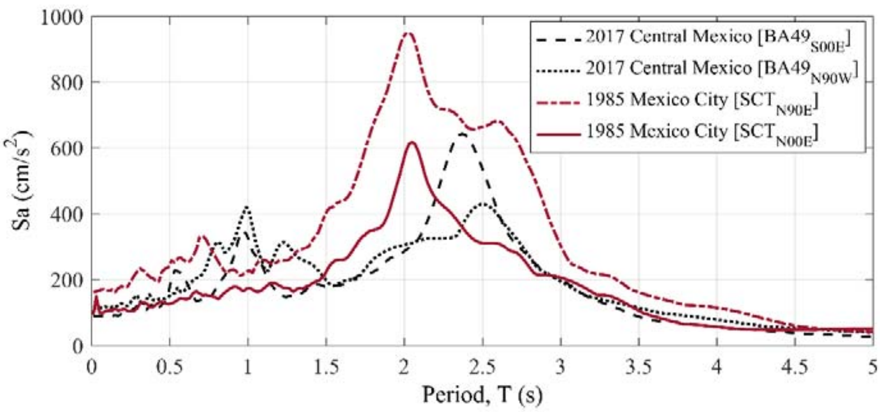

Figure 2. Comparison between the response spectra (5% damped) of the horizontal as-recorded components from the 1985 Mexico City earthquake (SCT station – seismic zone III C) and the 2017 Central Mexico earthquake (BA49 station – seismic zone III C). The color version of this figure is only available in the electronic edition.

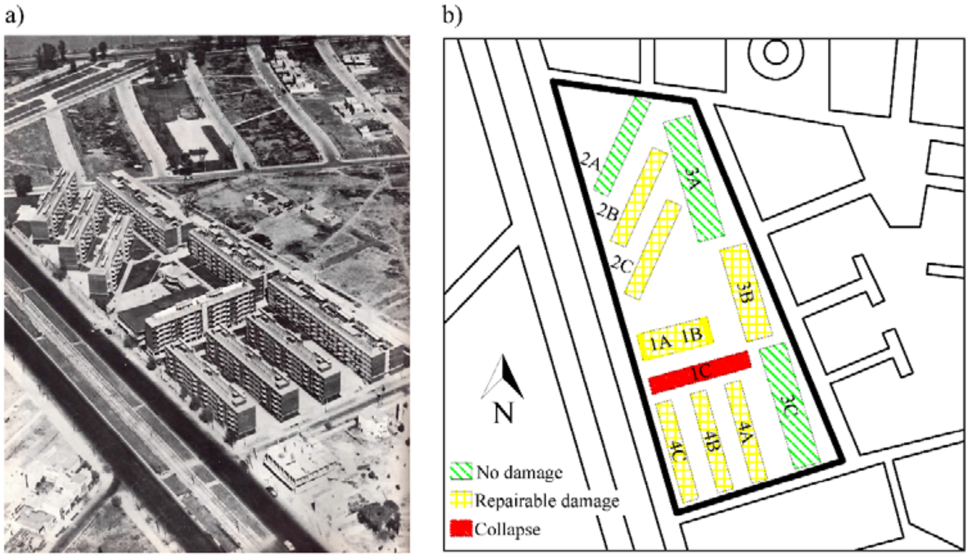

Figure 3. a) ISSSTE multifamily complex development, Tlalpan, Mexico City, 1957 (see Data and Resources). b) Plan view of the complex. Damage levels in the complex are shown. The color version of this figure is only available in the electronic edition.

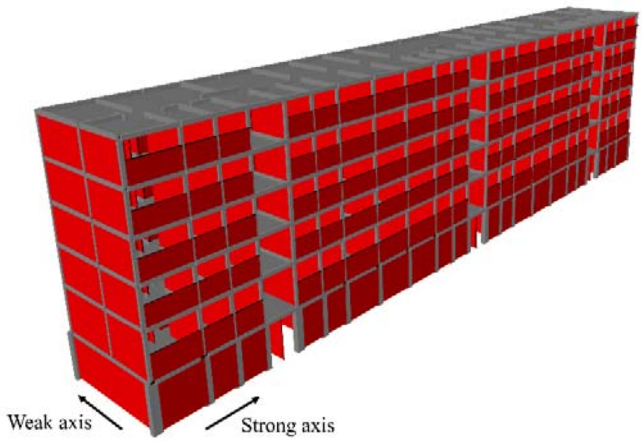

Figure 4. 3D building model.

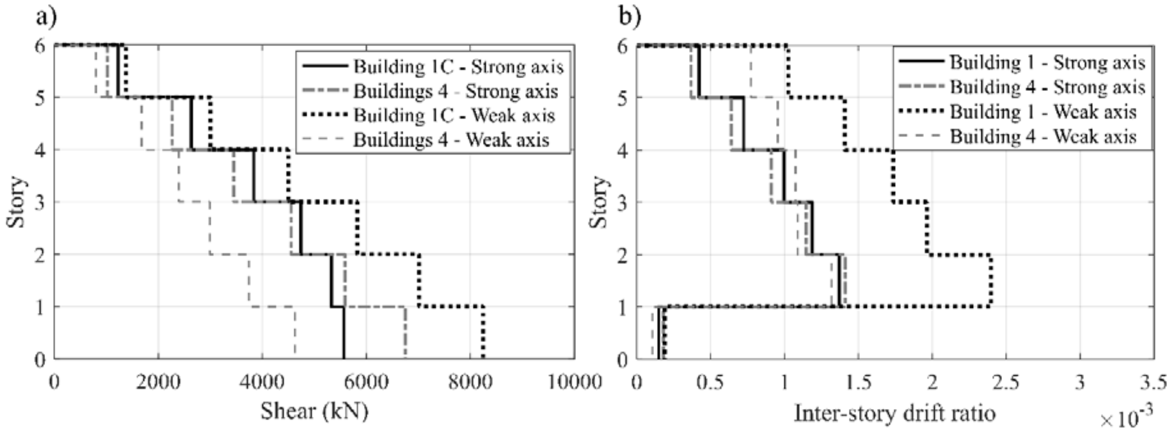

Figure 5. (a) Shear and (b) inter-story drift comparison between the 1C and 4A, B and C buildings obtained through the time-history analysis with the ground motion of the DX37 station.

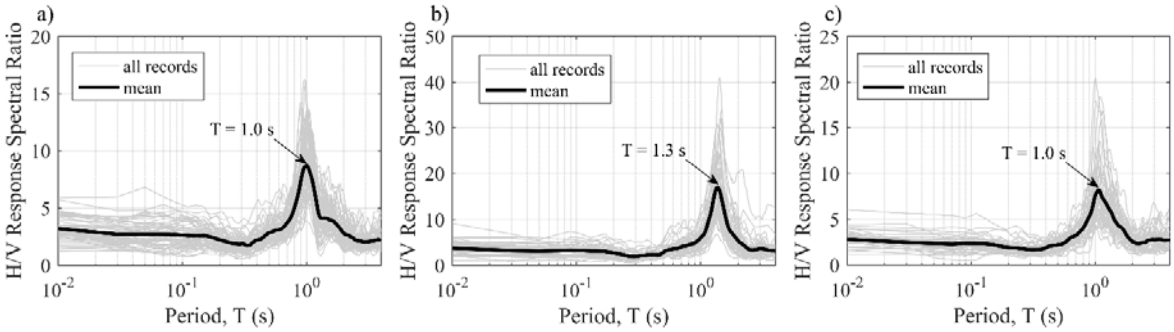

Figure 6. H/V response spectral ratios for the strong-motion stations (a) DX37, (b) CH84, and (c) AO24.

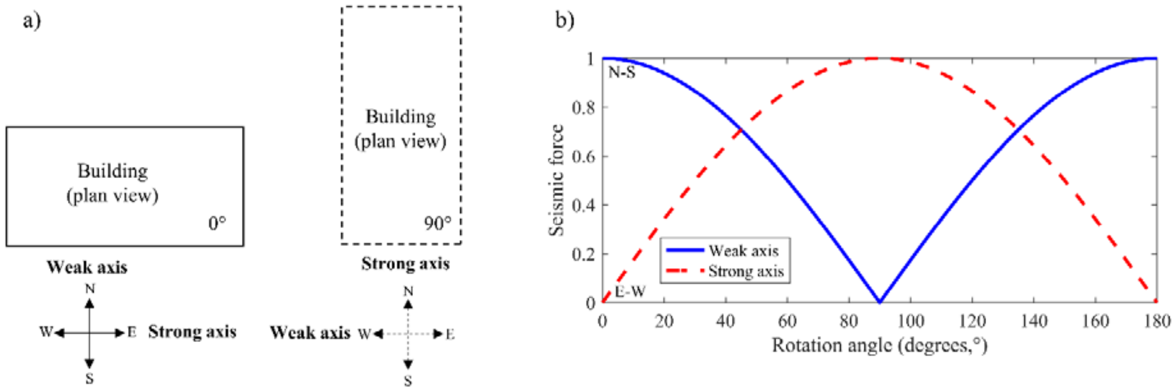

Figure 7. (a) Strong and weak axes of a building and (b) effective seismic forces affecting the strong and weak axes, as a function of the rotation angle. The color version of this figure is only available in the electronic edition.

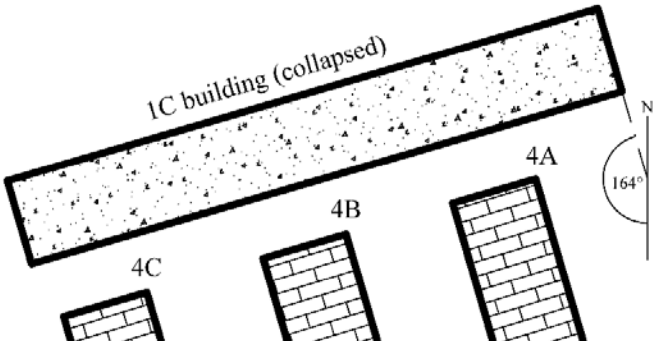

Figure 8. The azimuth of the 1C building measured from the south.

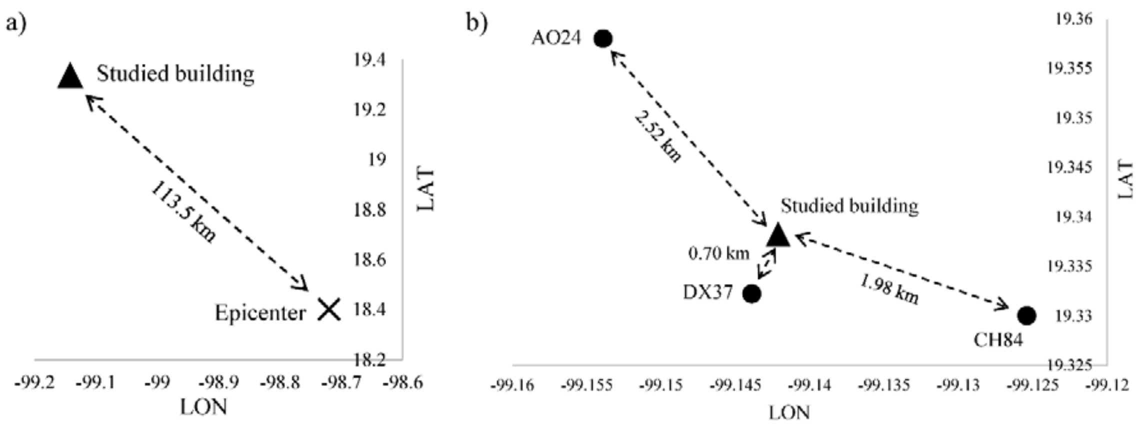

Figure 9. a) Epicentral distance from the 2017 Central Mexico earthquake to the 1C building. b) The three accelerographic stations closest to the 1C building site.

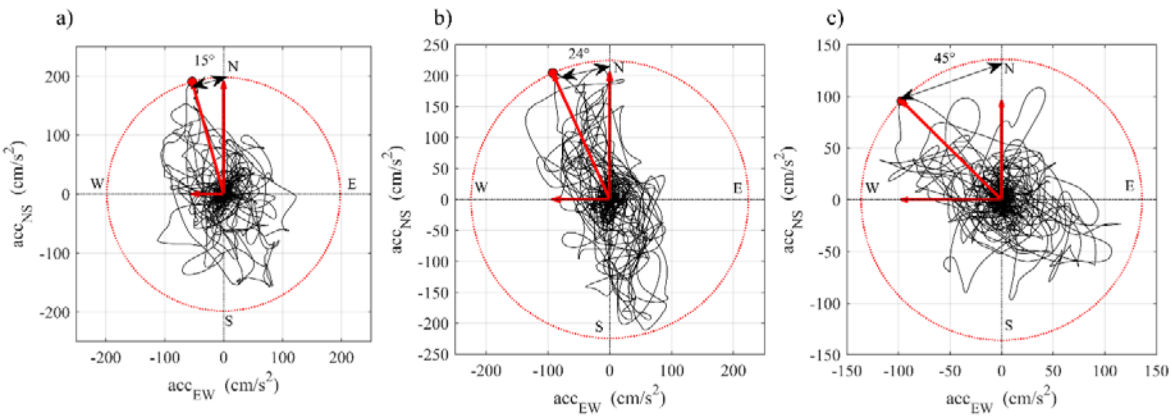

Figure 10. Particle acceleration motions at the three accelerometric stations closest to the 1C building site: (a) DX37 station, (b) CH84 station, and (c) AO24 station. The color version of this figure is only available in the electronic edition.

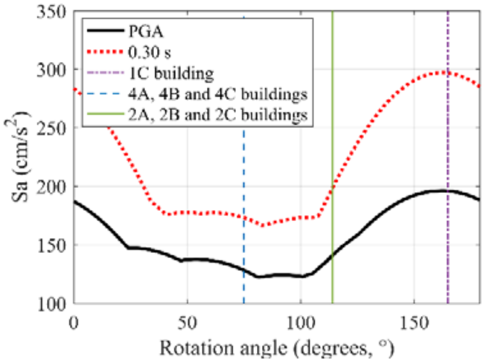

Figure 11. Variation of PGA and spectral acceleration, Sa, of a single-degree-of-freedom 5% damped oscillator with T=0.3 s as a function of the orientation angle, at DX37 accelerographic station. Vertical lines indicate the azimuths, measured from the south, to the weak axis of the 1 (C), 2 (A, B and C), and 4 (A, B and C) buildings. The color version of this figure is only available in the electronic edition.

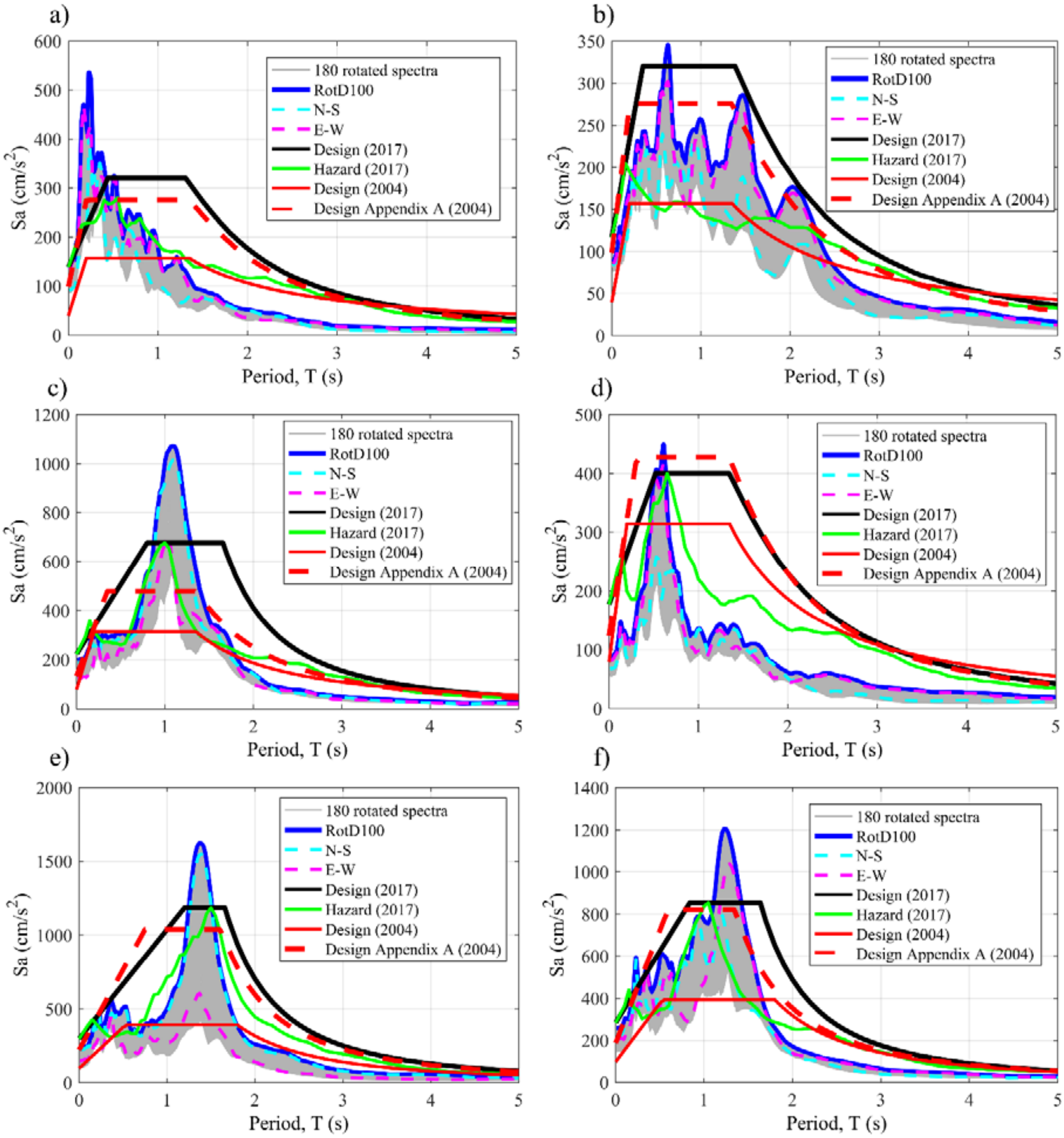

Figure 12. Comparison of response spectra of records at different accelerometric stations in Mexico City, during the 2017 Central Mexico earthquake: (a) CP28 station [zone I], (b) PA34 station [zone I], (c) DX37 station [zone II], (d) EO30 station [zone II], (e) CH84 station [zone IIIA], and (f) JC54 station [zone IIIA]. The color version of this figure is only available in the electronic edition.

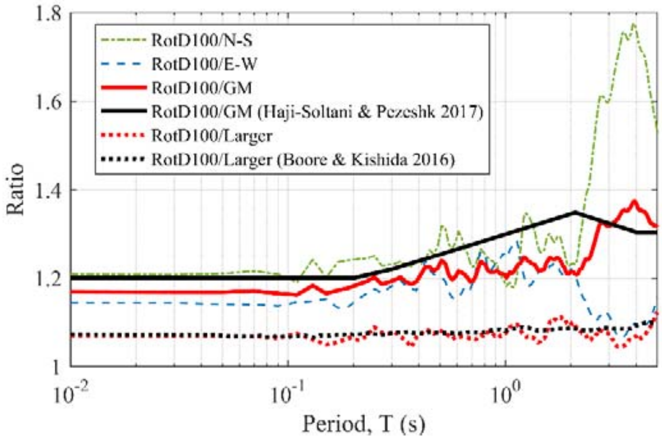

Figure 13. Comparison of the ratios RotD100/N-S, RotD100/E-W, RotD100/GM, and RotD100/Larger with ratios proposed by other researchers. The color version of this figure is only available in the electronic edition.

Appendix

This Appendix shows a summary of the results obtained from the analysis of the response spectra in Tables A1 to A6.

Table A1 Seismic zone I.

Station	Epi. [km]	PGA N-S [cm/s^2]	PGA E-W [cm/s^2]	PGA Z [cm/s^2]	Soil Period [s]	Exceed 2004	Exceed App. A. 2004	Exceed 2017
CE18	111.3	72.7	51.1	29.7	0.50	**Yes**	No	No
CP28	121.6	90.3	133.4	81.2	0.50	**Yes**	**Yes**	**Yes**
CS78	119.9	87.0	55.5	58.0	0.50	**Yes**	**Yes**	**Yes**
FJ74	112.5	92.2	91.1	50.1	0.50	**Yes**	**Yes**	**Yes**
MT50	124.3	47.1	58.3	29.8	0.50	**Yes**	No	No
PA34	95.6	83.2	85.6	60.0	0.50	**Yes**	**Yes**	**Yes**
TP13	110.0	60.3	66.6	51.6	0.50	**Yes**	No	No
UI21	122.1	74.7	79.3	35.5	0.50	**Yes**	**Yes**	No

Table A2 Seismic zone II.

Station	Epi. [km]	PGA N-S [cm/s^2]	PGA E-W [cm/s^2]	PGA Z [cm/s^2]	Soil Period [s]	Exceed 2004	Exceed App. A. 2004	Exceed 2017
AO24	115.9	106.4	119.7	47.9	0.94	**Yes**	No	No
AU46	119.1	77.3	94.9	33.4	0.90	**Yes**	No	No
CO47	117.9	72.0	94.0	30.6	0.73	**Yes**	No	**Yes**
DR16	131.7	71.0	77.2	25.1	0.63	**Yes**	**Yes**	No
DX37	112.8	187.7	123.9	52.4	0.73	**Yes**	**Yes**	**Yes**
EO30	120.0	67.5	82.1	34.5	0.67	**Yes**	**Yes**	**Yes**
ES57	121.3	70.5	83.9	28.2	0.73	**Yes**	No	No
GR27	128.9	84.7	119.6	44.8	0.76	**Yes**	**Yes**	No
LV17	128.9	123.0	104.1	25.9	0.63	**Yes**	**Yes**	No
ME52	125.3	62.8	72.2	31.7	0.77	No	No	No

Table A3 Seismic zone IIIA.

Station	Epi. [km]	PGA N-S [cm/s^2]	PGA E-W [cm/s^2]	PGA Z [cm/s^2]	Soil Period [s]	Exceed 2004	Exceed App. A. 2004	Exceed 2017
CH84	111.9	225.6	149.0	83.8	1.35	**Yes**	**Yes**	**Yes**
IB22	113.6	119.0	160.9	46.2	1.41	**Yes**	No	No
JC54	110.2	220.3	204.1	59.9	1.11	**Yes**	**Yes**	**Yes**
MI15	107.1	207.2	133.4	55.3	1.24	**Yes**	**Yes**	**Yes**
SI53	117.4	129.0	177.6	56.8	1.31	**Yes**	No	**Yes**
UC44	124.1	125.3	124.9	41.7	1.26	**Yes**	No	No

Table A4 Seismic zone IIIB.

Station	Epi. [km]	PGA N-S [cm/s^2]	PGA E-W [cm/s^2]	PGA Z [cm/s^2]	Soil Period [s]	Exceed 2004	Exceed App. A. 2004	Exceed 2017
AL01	123.5	117.1	108.6	40.2	1.77	**Yes**	No	No
BL45	122.6	102.3	114.5	39.7	2.22	No	No	No
CI05	122.6	113.3	114.2	51.2	2.09	**Yes**	No	No
CJ03	121.3	112.0	98.0	36.4	1.75	**Yes**	No	No
CJ04	121.3	123.9	97.1	34.8	1.75	**Yes**	No	No
CO56	122.6	109.8	114.0	53.8	2.04	**Yes**	No	No
GA62	123.6	97.1	84.0	33.7	1.88	**Yes**	No	No
GC38	109.7	125.6	124.2	43.2	1.42	**Yes**	No	No
LI58	123.0	95.8	89.9	51.1	1.97	**Yes**	No	No
PE10	117.4	101.4	124.6	31.1	2.02	**Yes**	No	No
RM48	122.9	61.1	78.0	37.9	2.44	No	No	No
SP51	115.3	77.4	100.4	38.5	1.78	No	No	No
TL08	124.6	82.8	81.2	30.2	1.74	No	No	No
TL55	125.3	82.5	69.2	33.6	1.47	No	No	No
VG09	124.6	119.5	101.8	36.4	2.17	**Yes**	No	No

Table A5 Seismic zone IIIC.

Station	Epi. [km]	PGA N-S [cm/s^2]	PGA E-W [cm/s^2]	PGA Z [cm/s^2]	Soil Period [s]	Exceed 2004	Exceed App. A. 2004	Exceed 2017
AP68	116.4	115.2	133.9	81.4	2.75	**Yes**	No	No
BA49	120.8	88.9	113.2	30.6	2.34	**Yes**	No	No
BO39	125.2	77.9	95.1	24.1	2.52	**Yes**	No	No
CA59	121.5	83.5	89.8	35.6	2.70	No	No	No
CU80	107.3	144.1	168.3	41.7	2.50	**Yes**	No	No
HJ72	121.9	90.3	96.4	40.6	2.50	**Yes**	No	No
JA43	119.6	82.9	106.3	47.8	2.67	**Yes**	No	No
MY19	110.6	119.9	111.6	85.4	2.54	**Yes**	No	No
RI76	123.1	52.4	72.7	24.2	3.08	No	No	No
VM29	117.1	85.2	94.8	35.9	2.28	**Yes**	No	No
XO36	104.9	124.1	173.6	50.5	2.25	**Yes**	**Yes**	No
XP06	121.5	81.7	108.2	31.0	2.47	**Yes**	No	No

Table A6 Seismic zone IIID.

Station	Epi. [km]	PGA N-S [cm/s^2]	PGA E-W [cm/s^2]	PGA Z [cm/s^2]	Soil Period [s]	Exceed 2004	Exceed App. A. 2004	Exceed 2017
AE02	119.8	96.2	114.9	42.2	4.54	**Yes**	No	No
AU11	116.9	72.1	90.5	35.2	3.63	**Yes**	No	No
CE23	123.5	52.1	60.0	26.5	4.17	No	No	No
CE32	115.1	80.4	76.8	35.8	2.92	**Yes**	No	No
DM12	121.3	87.5	90.5	41.0	3.25	**Yes**	No	No
PD42	118.7	83.8	96.3	42.4	3.43	**Yes**	No	No
TH35	102.0	189.9	186.7	59.0	4.00	**Yes**	**Yes**	No